Enhancement of critical current density using electro-deposited micro porous structure

S.Y. Park[a], D.H. Park[a], H. Park[b] and B.J. Chung[a*]
[a]*Department of Nuclear Engineering, Kyung Hee University*
1732 Deogyeong-daero Giheung-gu Yongin-si Gyeongg-do 17104, Republic of Korea
[b]*School of Energy Engineering, Kyungpook National University*
80 Daehak-ro, Buk-gu, Daegu, 41566, Republic of Korea
clappingy01@khu.ac.kr, q345ert@khu.ac.kr, hkyunp@knu.ac.kr, bjchung@khu.ac.kr

***Keywords: CHF, CCD, Porous structure, Electrodeposition**

1. Introduction

Beyond a certain high heat flux, known as critical heat flux (CHF), unstable vapor films are formed on the heated surface. They significantly impair heat transfer, which results in a sudden increase in the surface temperature [1]. Hence, numerous studies are being performed to delay the CHF phenomenon. However, the boiling experiments often encounter extreme conditions, leading to a failure of experimental equipment and measurement devices. To address this challenge, our research group has been exploring an alternative experimental technique to simulate the CHF.

Fig. 1 depicts the boiling curve in the boiling system and E-I curve in the hydrogen evolving water electrolysis system. The wall superheat and heat flux in the boiling system correspond to the voltage and current density in the water electrolysis system, respectively. Similar to the CHF, an N-shaped curve can be obtained due to the formation of the hydrogen film on the cathode surface. The ridge at the E-I curve has been known as critical current density (CCD).

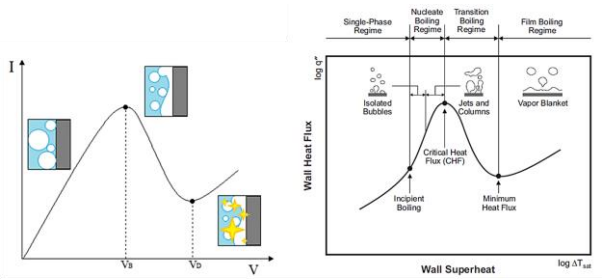

(a) V-I curve in a water electrolysis (b) Pool boiling curve in a boiling system

Fig. 1. Similarity between water electrolysis and boiling system (a) E-I curve in water electrolysis [2]. (b) Pool boiling curve in boiling system [1].

It was confirmed that the CCD mechanism can be explained by well accepted CHF models; macrolayer dryout and dry spot models. Furthermore, our group also confirmed that the influence of hydraulic parameters such as surface tension, inclination of the surface, and active area affects the CCD similarly to the CHF. The present work extends the scope to the influence of surface structure that is often employed to delay the CHF using electrodeposition to form a porous structure on the surface.

2. Existing study

Electroplating offers a cost-effective and simple method to form a porous structure. Copper electrodeposition using acid sulfate typically follows a two-step method. Fig. 2 illustrates a schematic image of this process. In the 1st step, a high current is applied for a short duration, resulting in the electroplating together with the hydrogen evolution. The hydrogen bubbles determine the size of a porous structure. Subsequently, the surface experiences a low current as the 2nd step, without hydrogen evolution so that copper adheres to the porous structure to strengthening it.

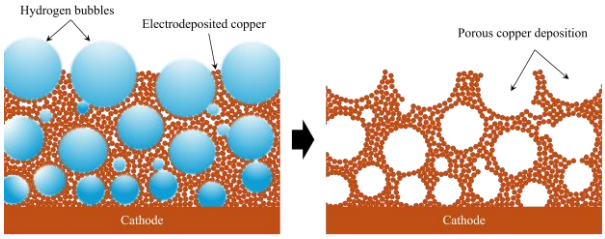

Fig. 2. Deposition of porous copper using hydrogen bubbles at templates.

Several studies have been conducted to investigate the influence of electrodeposition on the porous structure and its impact on the CHF. Genki and Ali [12] varied the current density in the 1st step and observed changes in the CHF and heat transfer coefficient (HTC) with the thickness of the structure. Patil et al. [13] figured out that the boiling performance was not significantly influenced by the deposition time in the second step. Nevertheless, the porous form, which varied with the 1st step current density, had a notable effect on the HTC, especially when exhibiting a cauliflower-like form. Gheitaghy et al. [14] conducted the boiling experiments by varying the temperature of the electrolyte and found that the boiling performance is excellent at the room temperature. The majority of the electro-deposition research focuses on varying experimental variables to find optimal conditions.

3. Experimental setup

3.1. Copper electro-deposition setup

Fig. 3 shows a schematic image of experimental apparatus and electrical circuit for the electro-deposition. 0.8 M $CuSO_4$ and 1.5 M H_2SO_4 solution is used. The cathode where the electro-deposition occurs was a 10 mm diameter disk. And a cylindrical copper was used as the counter electrode (anode). Prior to the deposition, the cathode was cleaned by DI water and isopropyl alcohol (IPA). The current was modulated directly on power supply (DW INSTEK GEP112178). After then, the micro-porous deposited surface was washed by DI water and dehydrated using a heat gun.

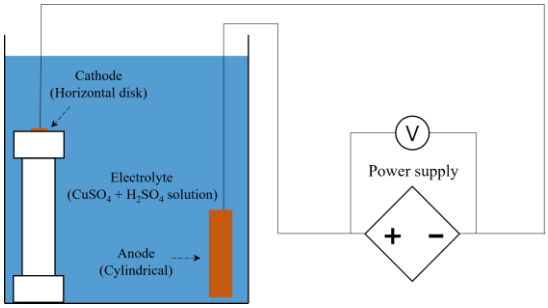

Fig. 3. Schematic experimental apparatus and electric circuit of electro-deposition.

Table 2 shows the test matrix of this experiments. The current density in the 1st step was varied from 3–30 kA/m^2, while the 2nd current density and deposition time was fixed to neglect of 2nd step effect. After the experiments, the surface was captured by scanning electron microscopy (SEM) and analyzed using ImageJ software to measure porous layer characteristic parameters (porosity, porous diameter, and porous thickness).

Table. 1. Test matrix for this experiment.

Solution	Current density (kA/m^2)			Deposition time (s)
0.8 M $CuSO_4$ + 1.5 M H_2SO_4	1st step	Case 1	3	15
		Case 2	5	
		Case 3	7	
		Case 4	15	
		Case 5	20	
		Case 6	30	
	2nd step	1		180

3.2 Water electrolysis CCD experiments setup

Fig. 4 is a schematic image for experimental apparatus and electric circuit for the CCD experiments. The 1.5 M H_2SO_4 solution was used for the working fluid. The plain and electro-deposited 10 mm diameter copper surfaces were used as cathodes where hydrogen evolution occurred. And 100×200 mm rectangular copper was used for the counter electrode. The electric potential was applied using DC power supply (Keysight N8965) and the voltage and current data were recorded by data acquisition (DAQ) system.

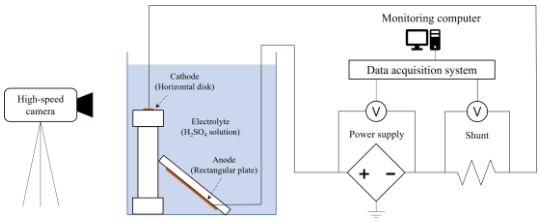

Fig. 4. Schematic image of hydrogen evolving experimental apparatus and electric circuit.

A time duration of ~ 5 s was required at each voltage step to get the stable data. Three repetitive experiments were performed for each case, and the final data were calculated by averaging the results. The CCD was determined by averaging 100 data before the current suddenly dropped and the hydrogen generation rate (HGR) of was determined as inclination of normal electrolysis regime as shown in Fig. 5. During the experiments, the hydrogen bubble behaviors was recorded by high-speed camera (Phantom Lab 11 6Gmono Komi) with 1000 frame per second.

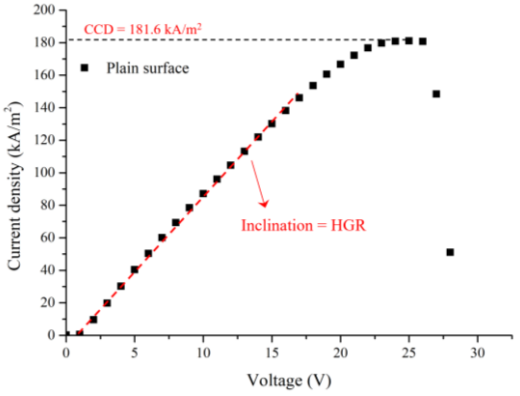

Fig. 5. E-I curve of plain surface with HGR and CCD.

4. Result and discussion

4.1. Examination of the porous surface

The porous structure formed by electro-deposition method was examined by investigating SEM images. The quantified data are presented in Table 2. As the current density in the 1st step increased, both the average pore diameter and thickness increased. The size of hydrogen bubbles generated during the initial electroplating step is determined by the pressure difference between liquid and vapor. Hence, as the applied current density raises the pressure of vapor, the bubble size follows increases [15]. Moreover, since the

amount of the deposited copper increased with the increased current density, the pore thickness increased.

Furthermore, the porous structures are classified based on their geometric configuration. In the Case1–3, open disk pores with a single-layer structure are observed as shown in Fig. 6 (a-c). Due to insufficient current density to form hydrogen bubbles, their pore boundaries are incomplete. Moreover, since the amount of deposited copper is insufficient, the plain copper surface was observed at the bottom of the pore, as illustrated in fig. 7(a). Conversely, reentrant pores with multi-layer structure were observed for Case 4–6 as shown in Fig. 6(d–f). The current density in these cases was sufficient to generate an ample amount of hydrogen bubbles, resulting in a distinct pore outline. Additionally, several small pores were formed inside the larger pore instead of exposing the cathode surface. The formation of these multiple layers is attributed to the adequate amount of electrodeposited copper. Furthermore, the small pores within the porous structures were interconnected with the larger one.

Table. 2. Quantification data about pore diameter, layer thickness, and porosity for Case 1-6.

	Averaged pore diameter (μm)	Averaged pore thickness (μm)	Porosity
Case 1	50.5 ± 12.6	138.7 ± 12.7	0.885
Case 2	56.0 ± 17.3	160.4 ± 20.8	0.871
Case 3	58.3 ± 19.3	170.6 ± 12.0	0.859
Case 4	98.2 ± 21.8	200.5 ± 5.9	0.811
Case 5	120.1 ± 22.6	205.2 ± 19.5	0.837
Case 6	103.4 ± 20.0	289.5 ± 22.5	0.814

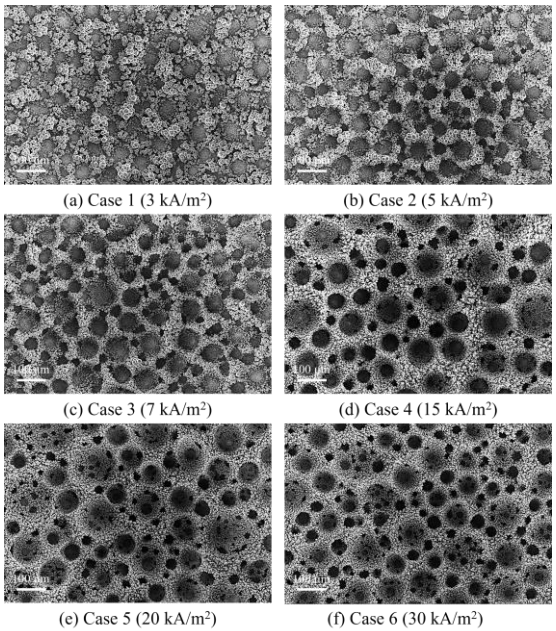

Fig. 6. SEM images of six electrodeposited porous surfaces with different morphogenic construction.

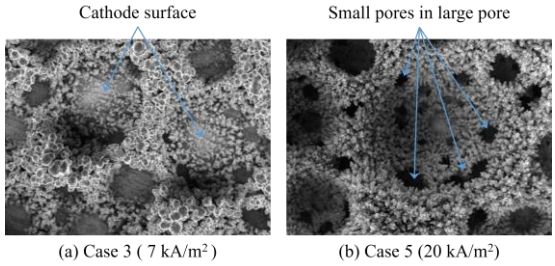

Fig. 7. Difference between single layer and multi-layer electro-deposited porous structures.

4.2. Influence of porous structures on CCD

Similar to the CHF results [12–14], the micro porous structures influence on the CCD and HGR significantly. Fig. 8 depicts the E-I curves in this experiment. In all cases electro deposited surface exhibited an enhanced HGR and CCD compared to the plain surface. The enhancement rate was quantified in Table 3. The increase in HGR is attributed to the increased the nucleation site density of porous surface [16]. Additionally, the porous structure promotes capillary wicking, thereby increasing the bubble generation frequency [17]. To achieve CCD, partial films should be formed on the active surface. Since the capillary wicking facilitates the liquid supply on the cathode surface, the growth of dry pots beneath the film is hindered, resulting in a delay of CCD.

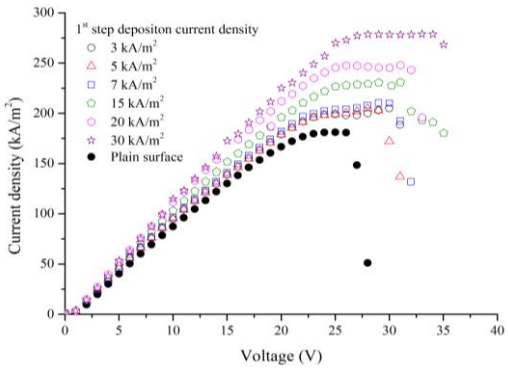

Fig. 8. Variation of E-I curves according to the 1st step current magnitude.

Table. 3. Enhancement rate of CCD and HGR about flat plate cathode.

	CCD enhancement (%)	HGR enhancement (%)
Case 1	12.6	7.8
Case 2	12.8	6.5
Case 3	16.3	8.6
Case 4	27.4	15.6
Case 5	36.9	25.3
Case 6	54.0	29.6

4.3. Form of porous structure influence to hydrogen evolving

As mentioned in section 4.1, Case 1–3 and Case 4–6 exhibit distinct forms of porous structures. In case of Case 1–3, the CCD enhancement rate was lower than 16 %, while Case 4–6 shows a higher enhancement rate exceeding 27 %. Furthermore, the HGR enhancement for cases 1–3 remains below 10 %, whereas for Case 4–6, it ranges between 15 to 30 %. These differences stem from variations in the pore shape such as open disk and reentrant and layer such as single and multi-layer of each form of porous structure.

Compared to the open disk pore (Case 1–3), the reentrant cavities (Case 4–6) stably retain the bubble embryos even after bubble departure. Furthermore, in the multi-layer porous structure where the pores are interconnected, the active pores enable the adjacent inactive ones to active. For this reason, even at the same cell potential (wall superheat), the higher current density was observed in the Case 4–6 compared to the Case 1–3 as shown in Fig. 8.

Fig. 10 compares the bubble behaviors of Case 3 and 6 at same current density. The same current density means same hydrogen generation rate. In Case 6, the smaller bubbles generated more vigorously compared to the Case 3 due to the enhanced surface wettability.

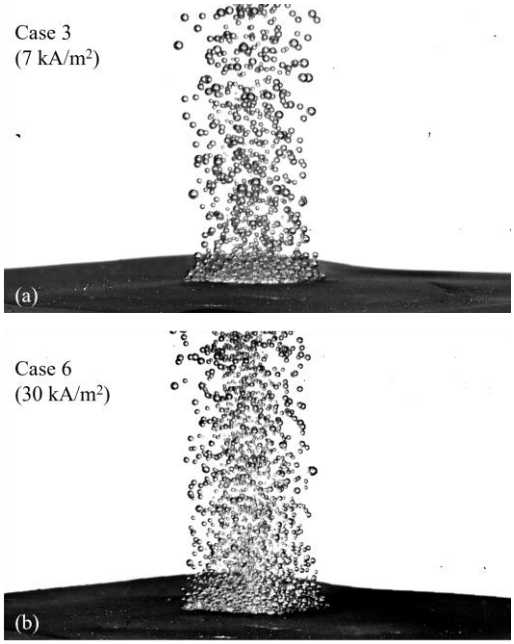

Fig. 10. Bubble difference between Case 3 and Case 6 at same current density (38 kA/m^2).

A set of droplet spreading experiment was performed to quantify relative wettability among the investigated surfaces. The spreading times were measured using high-speed camera by dropping 10 μL of solution (same as working fluid) just above each surface. As the porous structure developed, the spreading time becomes shorter. Porous structures with open disk pore and single layer exhibited longer spreading times ranging from 122 to 202 ms (Case 1 to 3). Conversely, with reentrant pore and multiple layer, the spreading time decreased ranging from 99 to 65 ms (Case 4 to 6). Hence, Case 6 showed smaller bubbles than that of the Case 3.

Fig. 11 compares the bubble behavior of Case 3 and 6 at just before CCD. In Case 3, the CCD occurred when the partial film was formed at the periphery of cathode surface as shown in Fig. 11(a). However, in Case 6, CCD occurred despite the absence of partial film on the periphery and the presence of small bubbles as shown in Fig. 11(b). Due to the smaller bubbles and increased capillary force in Case 6, the formation of partial film at the cathode periphery was interrupted. Consequently, the CCD is significantly delayed until the film is formed beneath the pores.

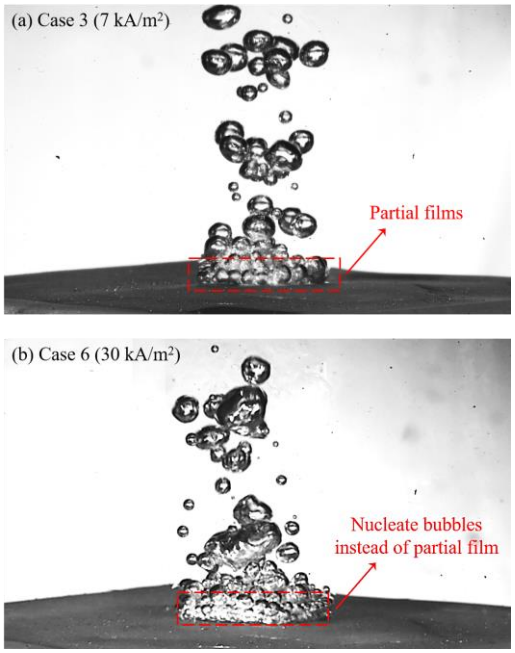

Fig. 11. Comparison of hydrogen bubble between Case 3 and Case 6 behaviors at just before CCD.

5. Conclusion

The present hydrogen evolution experiments using porous structure were performed to strengthen an analogous relation between the boiling system and the hydrogen evolving system. The 1st step deposition current density was varied to obtain distinct porous structure.

In all porous structure exhibits an enhanced bubble generation rate and CCD in all cases compared to the plain surface due to the increased nucleation site density and capillary wicking.

According to the 1st step deposition current magnitude, the distinct porous structures were observed. In the lower current cases, the single layer-open disk shape pores were observed while in higher cases, the

multi-layer reentrant shape pores were observed. Due to this morphology difference, smaller bubbles were generated more vigorously in higher current case which delay the CCD significantly.

From this result we confirmed that the influence of surface structure occurred in CCD similar to the CHF. Based on this result, the quantification of the influence of surface geometric structures on wettability (contact angle, capillary force etc.) will be performed.

REFERENCES

[1] G. Liang and I. Mudawar, Pool boiling critical heat flux (CHF) – Part 1: Review of mechanisms, models, and correlations, International Journal of Heat and Mass Transfer, Vol. 117, pp. 1352-1367, 2018.
[2] D.H. Park, H. K. Park, and B. J. Chung, Measurements of breakdown voltage and critical current density in a water electrolysis varying area and shape of working electrode., Journal of Electroanalytical Chemistry, pp. 928, 2023.
[3] S. M. Ohk, H. K. Park, and B. J. Chung, CHF experiments on the influence of inclination and gap size., International Journal of Heat and Mass Transfer, Vol. 132, pp. 929-938, 2019.
[4] H. K. Park and B. J. Chung, Simulation of Critical Heat Flux Phenomenon Using a Non-heating Hydrogen Evolving System., Frontiers in Energy Research, Vol. 7, 2019.
[5] H. K. Park and B. J. Chung, Comparison of bubble parameters between boiling and hydrogen evolving systems, Experimental Thermal and Fluid Science, Vol 112. 110316, 2021.
[6] H. K. Park and B. J. Chung, Comparative analysis of bubble behavior between boiling and hydrogen evolving system at horizontal cylinders, Heat and Mass Transfer, 2021.
[7] H. K. Park and B.J Chung, Application of microlayer dryout model for the critical current density of water electrolysis, International Communications in Heat and Mass Transfer, Vol. 130, 105759, 2022.
[8] H. K. Park and B. J. Chung, Estimation of critical number of hydrogen bubbles for critical current density using the dry spot model, Chemical Engineering Science, 249, 117344 (2022).
[9] J. W. Han, D. Y. Lee, H. K. Park, B. J. Chung, Experimental investigation on the flow CCD by analogically utilizing the CHF correlation, International Journal of Heat and Mass Transfer, 183, 122242 (2022).
[10] H. K. Park, J. W. Han, and B. J. Chung, Influence of hydrodynamic parameters on the critical current density at water electrolysis: Mass flux, channel inclination and inlet void fraction, International Journal of Hydrogen Energy, 47, 7535-7546, (2022).
[11] H. Vogt, Heat transfer in boiling and mass transfer in gas evolution at electrodes – The analogy and its limits, International Journal of Heat and Mass Transfer, 59, 191-197, (2013).
[12] M.S El-Genk and A. F. Ali, Enhanced nucleate boiling on copper micro-porous surfaces, International Journal of Multiphase Flow, Vol. 36, Issue 10, pp. 780-792, 2010.
[13] C. M. Patil, K. S. V. Santhanam, and S. G. Kandlikar, Development of two-step electrodeposition process for enhancing pool boiling, International Journal of Heat and Mass Transfer, Vol 79, pp. 989-1001, 2014.
[14] A. M. Gheitaghy, H. Saffari, D. Ghasimi, and A. Ghasemi, Effect of electrolyte temperature on porous electrodeposited copper for pool boiling enhancement, Applied Thermal Engineering, Vol. 113, pp. 1097-1106, 2017.
[15] H. Qui, K. Obata, Z. Yuan, T. Nishimoto, Y. Lee, and K. Nagato, Quantitative Description of Bubble Formation in Response to Electrolyte Engineering, Lagmuir, Vol. 39, Issue 14, pp. 4993-5001, 2023
[16] G. Liang and I. Mudawar, Review of pool boiling enhancement by surface modification, International Journal of Heat and Mass Transfer, Vol. 128, pp. 892-933, 2019.
[17] H. S. Ahn, C. Lee, J. Kim, and M. H. Kim, The effect of capillary wicking action of micro/nano structures on pool boiling critical heat flux, International Journal of Heat and Mass Transfer, Vol. 55, pp. 89-92, 2012.